ELSEVIER

Journal of Nuclear Materials 306 (2002) 85–98

journal of nuclear materials

www.elsevier.com/locate/jnucmat

Transport properties of zirconium alloy oxide films

H. Frank *

Department of Solid State Engineering, Faculty of Nuclear Sciences and Physical Engineering, Czech Technical University, Trojanova 13, 120 00 Prague 2, Czech Republic

Received 26 October 2001; accepted 16 May 2002

Abstract

The conductivity mechanism of oxide films on tubes of various zirconium alloys grown in water and steam was investigated by *I–V* measurements. Electrodes of Ga, Ag, graphite and Au gave different results. The current decrease at voltage application was due to formation of space charge, which could be extracted again as short-circuit current. The positive branch of the *I–V* characteristics could be fitted by a second-order polynomial. Neither the Schottky emission mechanism nor the Poole–Frenkel effect could be proved. A high invariable carrier concentration with extremely low, but temperature dependent mobility could be proved using the Mott–Guerney relation. The carriers originate from oxygen vacancies in a substoichiometric black oxide layer near the metal–oxide interface. The conduction mechanism is believed to be a hopping process of electrons between oxygen-vacancy traps. There exists a small ionic conduction part, building up an open-circuit voltage so that the *I–V* characteristics do not pass through the origin. The Meyer–Neldel rule applies.

1. Introduction

Zirconium alloys with enhanced corrosion resistance are used in nuclear light-water reactors as fuel cladding and channel box materials [1,2]. In a high-temperature aqueous environment, oxides are formed by diffusion of oxygen ions through the built-up layer, combining with zirconium ionized by electron emission [3]. Thus the oxidation of zirconium depends on the transfer of electrons from the metal to water, oxygen ions diffusing in the opposite direction. Therefore, the corrosion rate depends largely on the electron motion, which is governed by the electrical conductivity of the oxide layer. It is therefore of interest to investigate the electrical transport properties of the oxide layers with regard to the oxide-forming capability and assessment of corrosion resistance.

The excellent corrosion resistance of the alloys in aqueous solution is attributed to the formation of a passive film on the surface. Lee et al. [4] investigated the passive film on Zircaloy-4 by a photo-electrochemical method. The oxide consisted of an inner anhydrous layer with a band gap of 4.30 eV, and an outer hydrous ZrO_2 layer with a band gap of 2.98 eV.

Cox [5] found that the electronic conductivity is controlled by small amounts of alloying elements. Howlader et al. [3] concluded that electron conduction dominates the electrical conductivity of Zircaloy oxide films. They measured the electrical conductivity and *I–V* characteristics of Zircaloy oxide films over a wide temperature range using various electrode metals.

The oxide layer is not uniform, there exists a black hypostoichiometric layer of relatively higher conductivity near the oxide–metal interface, whereas the outer layer is white and of high resistivity, as could be shown metallographically by Cox et al. [6].

It is well known [3,7,8] that bulk ZrO_2 is predominantly an electronic high-resistivity semiconductor with a certain amount of ionic conduction at higher

* Tel.: +420-2 2435 8559; fax: +420-2 2191 2407.
E-mail address: kipl@troja.fjfi.cvut.cz (H. Frank).

0022-3115/02/$ - see front matter © 2002 Published by Elsevier Science B.V.
PII: S0022-3115(02)00879-6

temperatures [3]. The band gap is approximately 5 eV, work function 4.0 eV and relative permittivity 22. The observed activation energy is determined by the distance between the trap levels and the lower edge of the conduction band [9].

2. Experimental

Tube sections specimens 30 mm long and of 9 mm outer diameter prepared from the zirconium alloys Zr1Nb, ZIRLO and Zry-4W (Table 1) were oxidized in water at 360 °C and in steam at 500 °C; the oxide layer thickness lays between 2 and 200 μm dependent on oxidation temperature and exposure time. According to the outer appearance there were two kinds of specimens, namely samples with thin oxide layers of dark colour, and thick film samples with white oxide layers.

The samples were fitted with circular electrodes 6 mm in diameter at the oxide surface. Liquid Ga and colloidal silver paint applied with an Al tip were initially used, but Ga electrodes proved unstable, forming black scum at the oxide surface, and were therefore discarded. Silver paint electrodes and, subsequently, graphite sprayed-on electrodes, and finally vacuum evaporated gold electrodes, were found satisfactory and stable enough. Owing to the large contact area of 0.283 cm^2 guard rings appeared to be unnecessary, no difference was found with readings taken with and without guard rings. The specimens were mounted in a small thermostat, with a maximum temperature of 220 °C. The abraded front ends of the tubes of shining zirconium metal were in direct contact with pressed-on copper electrodes, on which a thermocouple was mounted for temperature control. The current was measured with a two-electrode arrangement, using only one contact to each electrode. The contact resistance between the copper electrode pressed onto the metallic bulk zirconium is certainly to be neglected, the same being true for the resistance between the metallic measuring electrode and the pressed-on 0.3 mm thick phosphorbronze contact spring. A voltage was applied to the zirconium metal. The Ga, Ag, Au or C surface electrode was earthed via a picoampere-meter with a resolution of 0.1 pA. To minimize thermal loading of the measuring contact, this was accomplished by means of the thin, 50 mm long contact spring, leading through a small opening in the thermostat wall. The voltage drop of the meter was mostly limited to 10 mV, with a possible maximum of 200 mV, which had to be subtracted from the source voltage for resistance calculations. The voltage supplied by a stable source could be varied from 0.1 to 100 V and was chosen with regard to the oxide layer thickness so as not to exceed the dielectric strength, with a maximum of about 4 MV/m. Normally the voltage was chosen as low as possible in order to remain basically within the linear part of the characteristics while ensuring good current reading. The I–V characteristics were measured at room temperature and at higher temperatures, ranging from 60 up to 220 °C with steps of 20 °C mostly with at least 10 positive and 10 negative voltage values. The voltage polarity is defined with respect to the bulk zirconium. Above room temperature a small short-circuit current and open-circuit voltage could usually be observed, due to the ionic conduction fraction. The temperature dependence of the resistivity was assessed either by measurements of the current at two constant but different potentials with slowly rising or decreasing temperatures with a rate of about 1 °C/min, or by measuring the complete characteristics at selected, constant temperatures. The electric current measurement was very time consuming, particularly in the room temperature range. The current on the application of voltage was much higher (up to 10-fold and more) than at equilibrium, which was reached only after a long time (up to several hours). At higher temperatures, such as 100 °C and more, it took only minutes to reach final steady-state values. The conductivity/resistivity was computed from the linear part of the I–V characteristics in the range of validity of Ohm's law. The activation energy E was derived from the slope of the $\log \rho = f(1/T)$ plot. The relative permittivity was calculated from the measured electrode capacity at 1000 Hz with known geometrical factors. There was virtually no hysteresis of the temperature-dependent currents when the readings were taken after waiting to reach equilibrium conditions. Measuring the current in the decreasing temperature mode starting from the temperature maximum (typically 100 °C) proved to be more convenient, shortening the idle time for steady-state readings.

Table 1
Chemical composition (wt%) of Zircaloys used in the present study

	Nb	Sn	Fe	Cr
Zr1Nb	1			
ZIRLO	1	1	0.1	
Zry-4W		1.3	0.2	0.1

3. Results and discussion

3.1. Time dependence of the electric current

The time dependence of the current after application of voltage $U = U_1$ at time t_0 is schematically indicated in Fig. 1. There flows a relatively high current, which decreases at first very fast and then gradually more slowly, until it reaches asymptotically its final value. This is due to charge carrier injection which builds up a space charge until the injection stops, and at equilibrium there

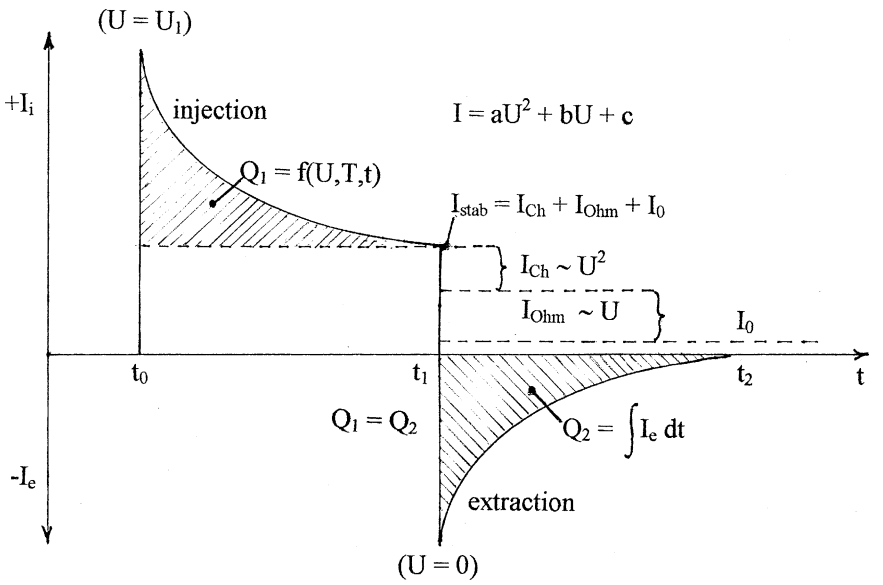

Fig. 1. Time dependence of injection current with turned-on voltage U_1 and extraction current without external voltage source.

flows a steady space-charge limited current. If the voltage is switched off at t_1 and the sample is shorted by the current meter, an extraction current of opposite polarity can be measured, the time integral of which equals the injected space charge. The extraction time $t_2 - t_1$ is practically the same as the injection time $t_1 - t_0$, and may take several hours at room temperature.

Typical behaviour of the gradual current decrease with time at different voltages is shown in Fig. 2. The current was highest at the moment of voltage application and then decreased slowly to reach asymptotically final equilibrium values. Evidently, this is a case of majority carrier injection building up a space charge. Equilibrium is reached when the space charge is high enough to stop further injection and a steady space-charge limited current is established. This is in agreement with Hartman et al. [9] who suggested, based on analogous calculations for silicon oxide films, that the conduction mechanism is due to bulk limited conduction, rather than to Schottky emission, as proposed by Simmons [12], or to the Poole–Frenkel effect, as suggested by Mead [13].

The existence of space charge accumulated by long-time injection currents was proved by measuring the short-circuit extraction currents flowing after completed injection, as shown by the dotted lines for $U = 0$ in Fig. 2. Due to the very low bulk conductivity, the injected charge remains virtually unchanged for a long time and can be extracted again. This extraction current decreases as a hyperbolic time function $I \sim t^{-n}$ with $1/2 > n > 2/3$ ($t^{-1/2}$ at 5 V and $t^{-2/3}$ at 100 V). The time integral of the extraction current equals the injected space charge. This is shown in Fig. 3 where the complete space charge, calculated by numeric integration of the time-dependent extraction current is plotted for three different injection voltages, giving a linear relationship. The calculated mean space charge density for this sample is 2×10^{-6} As/cm^3 V, or 1.2×10^{13} electrons/cm^3 V. Thus the oxide layer behaves like a storage cell, which can be charged and discharged.

Further measurements of the time dependence of the current were not carried out, as the measurement is very time consuming. It should be noted that the current at injection is larger than the short-circuit current at extraction by the amount of the steady-state current. This implies that the total current flowing at voltage application is composed of a constant equilibrium part, and a time-dependent injection current, building up the space charge. Therefore, meaningful current readings for conductivity determination cannot be taken until the space-charge forming process is completed and steady-state conditions for the space-charge limited current have been reached.

3.2. I–V characteristics

At space-charge limited current conditions, the I–V characteristics are non-linear and the total current I(stab), as indicated in Fig. 1, consists of three components, namely a space-charge limited part $I_{Ch} \sim U^2$, a linear part $I_{Ohm} \sim U$, and a constant short-circuit part I_0, which may be observed at higher temperatures. In this case the I–V characteristics do not pass through the origin. Neglecting higher powers of voltage, the positive branch of the characteristics can be approximated by a second-order polynomial

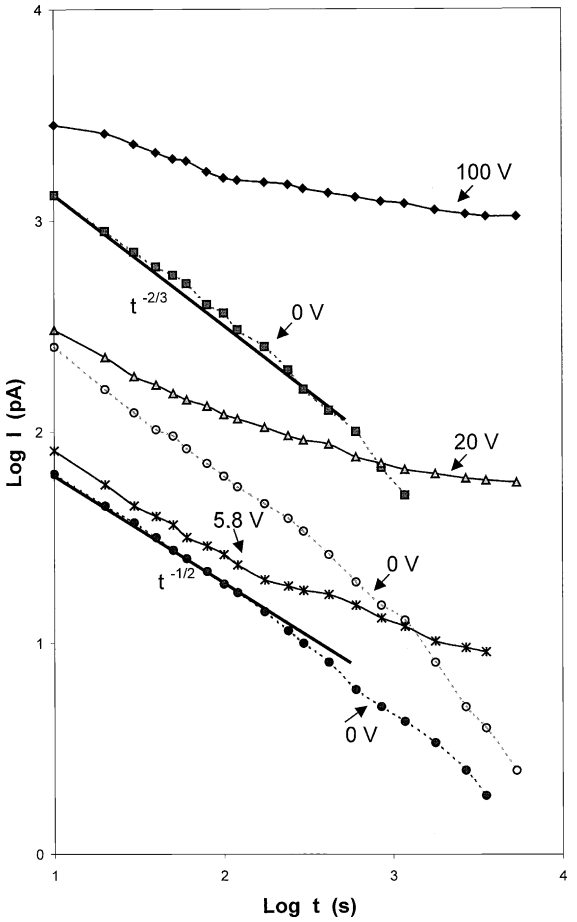

Fig. 2. (—): Time dependence of current after voltage turning on (charge injection). (- - -): Time dependence of the extraction current with the sample short-circuited by the pico-amperemeter. The time integral of the extraction current equals the previously injected charge. The current decreases hyperbolically, from $\sim t^{-1/2}$ at a low voltage to $\sim t^{-2/3}$ at higher voltages. Specimen: Zry-4W No. 3136057, room temperature.

$$I = aU^2 + bU + c, \tag{1}$$

where c is the short-circuit current. The linear term describes the current obeying Ohm's law, and $b = 1/R$ defines the resistance $R = \rho w/A$ of the sample with thickness w, contact area A and resistivity ρ. The quadratic term expresses the curvature of the characteristics and may be due to various mechanisms [9,10], namely

(a) Schottky type emission

$$J = AT \exp\left(\frac{e^{3/2}V^{1/2}}{kT\sqrt{\pi\varepsilon w}} - \frac{\Phi}{kT}\right), \tag{2}$$

(b) Poole–Frenkel mechanism

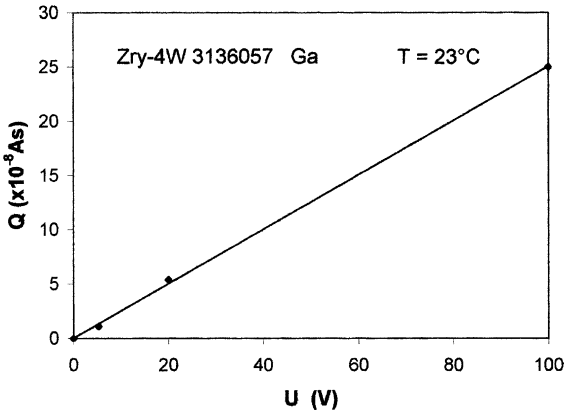

Fig. 3. Time integral of the extraction current (data from Fig. 2), showing a linear increase of the space charge Q with increasing injection voltage U.

$$J = G_0\left(\frac{V}{w}\right)\exp\left(\frac{2e^{3/2}V^{1/2}}{kT\sqrt{\pi\varepsilon w}} - \frac{X}{kT}\right), \tag{3}$$

(c) Space-charge limited current obeying Child's law [11] according to the Mott–Guerney relation [10]

$$J = \frac{9\varepsilon\varepsilon_0\mu}{8w^3}V^2, \tag{4}$$

where J is the current density, ε the permittivity and μ the mobility of the current carriers.

Here the evaluations are restricted to the positive branch (positive potential at the Zr bulk) because the characteristics are not only non-linear, but also asymmetrical.

The curvature of the characteristics is determined by the second-order term, which means that in addition to Ohm's law for the linear part, the second-order term according to Child's law manifests itself at higher voltages, Eq. (4).

Typical characteristics for positive voltage at the Zr electrode are shown in Fig. 4 (positive branches only). The sample was of the first kind with a thin layer (2.26 μm) of dark grey appearance. The characteristics were taken at constant temperature with voltage increments of 1 V each applied after 5 min up to 10 V with positive and then with negative polarity. Full lines of second-order polynomials are fitted to the measuring points according to Eq. (1)

Howlader et al. [3] attempted to explain the curvature of the I–V characteristics of Zircaloy oxide layers either in terms of Schottky emission or in terms of the Poole–Frenkel mechanism. They plotted the logarithm of current $\ln I$ as a function of the square-root of voltage $U^{1/2}$ for the Schottky emission model, and also as $\ln(I/U) = f(U^{1/2})$ for the Poole–Frenkel mechanism,

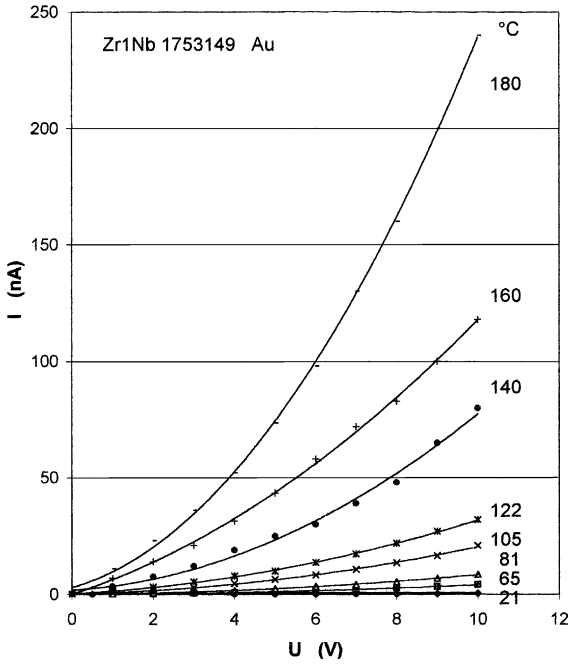

Fig. 4. Positive branch of non-linear I–V characteristics with fitted polynomials $I = aU^2 + bU + c$. Values of polynomial coefficients are in Table 2.

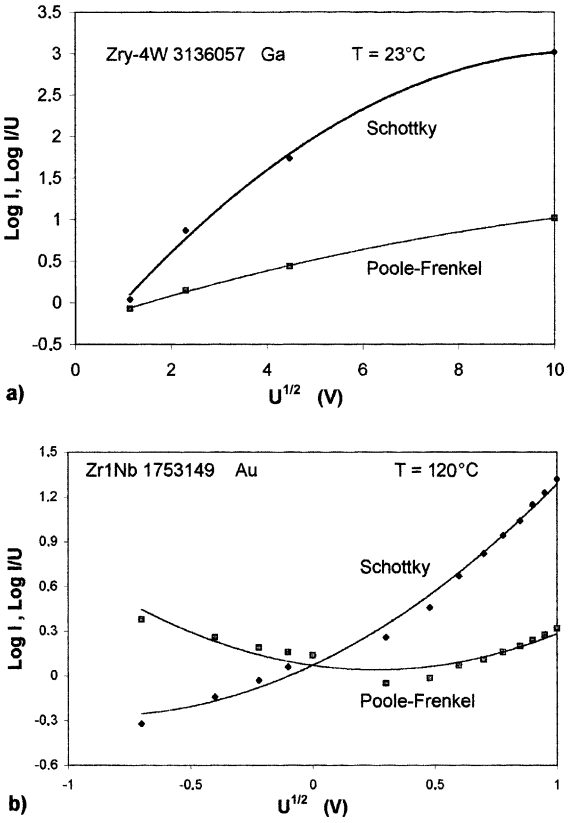

Fig. 5. Results of the I–V measurements plotted as $\log I = f(U^{1/2})$ and $\log I/U = f(U^{1/2})$; which should give straight lines for Schottky emission, or for Poole–Frenkel mechanism, respectively. (a) Results of Fig. 2, (b) thin layer, Zr1Nb 1753149, 120 °C, the measuring points for voltages higher than 0.5 V lie on straight lines as well for Schottky emission as also for Poole–Frenkel mechanism.

and obtained nearly linear relationships in either case. Our results plotted in Fig. 5(a) give curved lines not compatible with either Schottky emission or Poole–Frenkel mechanism, but the measuring points lie on straight lines in Fig. 5(b) at 120 °C and at voltages higher than 0.5 V.

The I–V characteristics are not only non-linear but also asymmetric. The current grows faster with increasing voltage when the potential at the Zr electrode is negative than when it is positive, which implies that the Zr–ZrO_2–M system has certain rectification capabilities. Since the work function of ZrO_2 is the same as that of Zr [3], no band bending takes place at this junction, and rectification to a certain extent can only be due to the work function difference between the oxide and the metallic measuring electrode, giving rise to band bending. A larger current flows if there is a positive potential at this electrode, which indicates that electrons are transferred. The forward direction of the carrier flow is consistent with electron motion. By virtue of Schottky's rule, current carrier transfer is easier from the semiconductor to the metal. Therefore electrons are the dominating charge carriers and ZrO_2 is an electronic semiconductor with space-charge limited current flow.

3.2.1. Evaluation of the second-order term

The coefficient of the quadratic term of the fitted polynomial to the measuring points of the positive branch of the I–V characteristics corresponds to Child's law and can be used to compute mobility and concentration of the free carriers. Table 2 gives the values of electron concentration and mobility at increasing temperatures for a Zr1Nb sample. Additional results are presented for samples of the other two Zircaloys in Fig. 6. It is astonishing that the electron concentration is very high and the mobility extremely low. Also the concentration is constant and independent of temperature. This is understandable, if we consider the high activation energy of about 1 eV for the conductivity. Therefore, only the mobility depending exponentially on temperature is responsible for the temperature dependence of conductivity.

Normally we should expect a decreasing mobility at higher temperatures due to electron–phonon interaction. The extremely low value of mobility in conjunction with its exponential temperature dependence indicates a hopping process to be responsible for electron transport.

Table 2
Temperature dependence of second-order polynomial coefficients, Eq. (1), and computed carrier concentration n and mobility μ

Temperature (°C)	a (nA/V^2)	b (nA/V)	c (nA)	n (cm^{-3})	μ (cm^2/V s)
Zr1Nb 1753149, Au (Fig. 4)					
21	0.00303	0.00799	0.0067	6.9×10^{14}	5.8×10^{-11}
65	0.0375	0.0266	0.061	2.5×10^{14}	5.4×10^{-10}
81	0.078	0.0507	0.146	2.5×10^{14}	1.03×10^{-9}
105	0.1173	0.3007	0.266	5.5×10^{14}	2.6×10^{-9}
122	0.215	1.07	0.178	1.05×10^{15}	4.7×10^{-9}
140	0.426	2.59	0.504	1.6×10^{15}	8.1×10^{-9}
160	0.693	5.34	0.04	1.9×10^{15}	1.4×10^{-8}
180	1.871	5.03	2.13	1.04×10^{15}	2.4×10^{-8}
	a (pA/V^2)	b (pA/V)			
Zry-4W 3136057, Ga (Fig. 2)					
23	0.09928	0.7173	–	1.1×10^{13}	3.1×10^{-9}

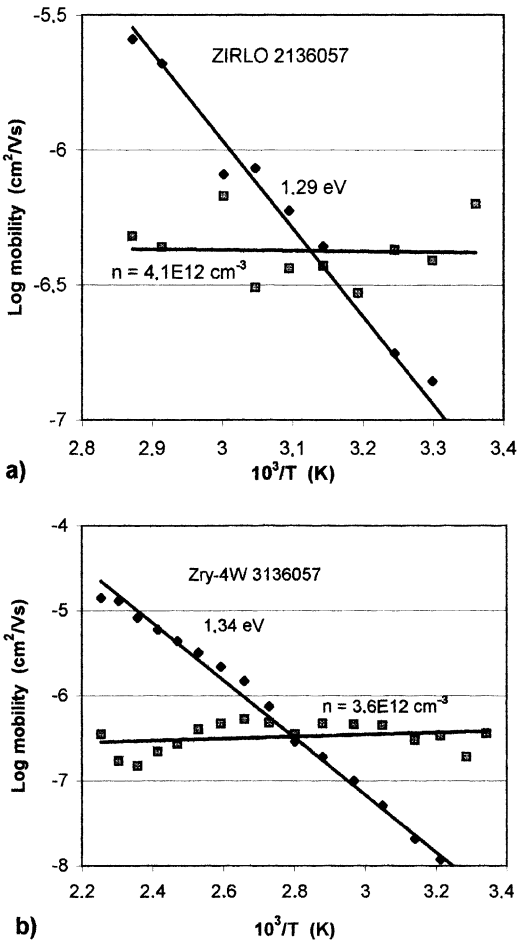

Fig. 6. Carrier concentration n and mobility μ, computed from the space-charge limited current part, using Eq. (4). Specimens: (a) Zry-4W 3136057, (b) ZIRLO 2136057. Points as measured. Straight lines computed from smoothed-out measurings.

Cox et al. [6] showed by metallographic investigation that the oxide film consists of a black, hypostoichiometric, highly conductive layer next to the oxide–metal interface, and a white oxide layer with high resistivity near the surface. We found that our specimens of smaller oxide layer thickness (<5 μm) were of dark colour (first kind), whereas specimens of thicker oxide layers were lightly coloured (second kind). It should be noted that the specimens of Zry-4W and ZIRLO (Fig. 6) are of the second kind of relatively large thickness (about 25 μm). The white, high resistivity oxide form outweighs the black, relatively high conducting form and explains the mean lower carrier concentration of about 4×10^{12} cm^{-3}. The Zr1Nb specimen in Table 2 is of the first kind of high conductivity, of dark colour, only 2.26 μm thick and has therefore a higher carrier concentration of 1×10^{15} cm^{-3}.

3.2.2. Evaluation of the linear term

The electrical conductivity can be evaluated from the observed current at known voltage only if Ohm's law is valid. The I–V characteristics must be determined in order to extricate the linear part. In other words, the constant b in Eq. (1) must be determined. There are two ways how to accomplish this. The first way is to measure currents I_1 and I_2 at different voltages U_1 and U_2. Assuming the characteristics behave according to Eq. (1), the constants a and b can then be calculated. The constant b is equal to the conductance, and with known geometrical factors A and w for the area and thickness, respectively, the conductivity can be calculated. Practically, this means that the current at first with U_1 must be measured with rising temperature, and then the measurement must be repeated at a different voltage U_2. It is difficult to get identical conditions for both measurements, therefore the other way is more adequate and consists in measuring the complete I–V characteristics at constant temperatures in the vicinity of the origin. Lim-

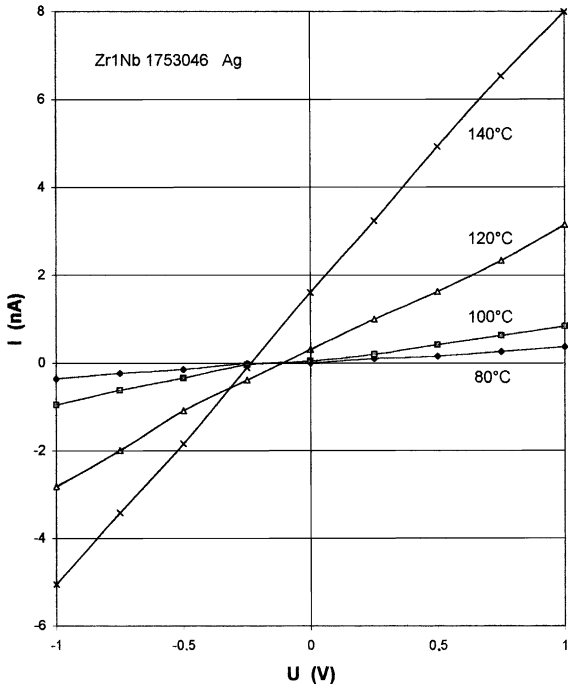

Fig. 7. Linear part of I–V characteristics measured around the origin. Specimen Zr1Nb.1753046 with Ag electrode, showing short-circuit current I_0 and open-circuit voltage U_0, temperatures 80–140 °C.

iting the voltage to low values within the linear part of the characteristics, the slope of the fitted straight line determines the conductivity/resistivity. This method is to be preferred to the extrapolation to zero voltage of the fitting of the complete large signal characteristics. Fig. 7 is a good example showing that the characteristics do not pass through the origin. There exist a short-circuit current I_0 at zero voltage and an open-circuit voltage $-U_0$ at zero current, both increasing with increasing temperatures.

3.2.3. Evaluation of the constant term

Owing to the small additional ionic conductivity in conjunction with the different work functions of Zr and the measuring electrode metal ($\Phi = 4.0$, 5.1, 4.3, 4.25 eV, for Zr, Au, Ag, Ga, respectively), we have basically an electrochemical cell with open-circuit voltage U_0 and short-circuit current I_0. This implies that the I–V characteristics do not pass through the origin; instead they intersect the voltage axis at $-U_0$, as shown in Fig. 7. In most cases, U_0 is only a few mV and can be neglected, but Zr1Nb specimens with thin oxide layers exhibited abnormally high open-circuit voltages.

There are several effects possible to explain the existence of open-circuit voltages, namely

(a) Photoelectric effect: Can be excluded, because the sample is mounted inside a light-tight box.

(b) Thermoelectrical effect: It must be stressed that the open-circuit voltage is definitely not of thermoelectric origin. The whole specimen is contained in the mini-thermostat at constant temperature. The zirconium bulk is connected with a thick pressed-on copper electrode ensuring good thermal and electrical contact. The currently used 0.3 mm thick and 50 mm long phosphor-bronze spring, contacting the measuring electrode on the oxide film, was exchanged for a copper wire 150 mm long and 0.1 mm thick with its whole length being inside the thermostat, so as to exclude any possible temperature gradient on the sample and its contacts, both of copper. No difference was found in readings with the normal spring contact and with the exchanged thin copper wire.

(c) Rectification of induced ac voltages: The ac heating current for the thermostat was exchanged for dc alimentation, and no difference was found in readings of the open-circuit voltage. Moreover the sample is completely screened by the thick copper walls of the thermostat, with only a short screened lead to the current meter. Measurement with an oscilloscope at the input of the pico-amperemeter revealed a 50 Hz disturbance of less than 2 mV only.

(d) Electrochemical action: The system Zr–ZrO_2–M could act like a fuel cell with open-circuit voltage exceeding 0.5 V. The zirconium metal instead of hydrogen is being oxidized by oxygen from the outside entering the oxide film by diffusion. By the oxidation process ZrO_2 originates instead of H_2O, thereby increasing the thickness of the oxide layer. This could be proved by measuring the capacitance of the system, which should decrease after prolonged flow of short-circuit current. Also the short-circuit current should stop in inert atmosphere without oxygen, and in a reducing atmosphere the short-circuit current should change sign. The polarity of the open-circuit voltage (and also of the current) is positive at the (gold) measuring electrode. This is in accordance with the polarity of a normal galvanic cell, where the dissolving zinc (here Zr) electrode is negative and the non-reacting graphite electrode is of positive polarity.

Shirvington [14] mentioned that the current flowing at zero potential represents the oxidation ionic current, which is exactly equal to the electron current. The temperature dependence of the open-circuit voltage of a typical specimen is shown in Fig. 8, exceeding 600 mV at 190 °C with the Au electrode, and without change of rising tendency. Using the Ag electrode, saturation of 360 mV was reached at temperatures over 160 °C. The voltage U_0 was measured by compensation of the short-circuit current. The latter can exceed 1500 pA depending on the electrode metal. Fig. 9 shows the temperature dependence of the short-circuit current I_0 for the same sample as shown in Fig. 8. The open-circuit voltage at 120 °C remained unchanged for 32 h. Although the

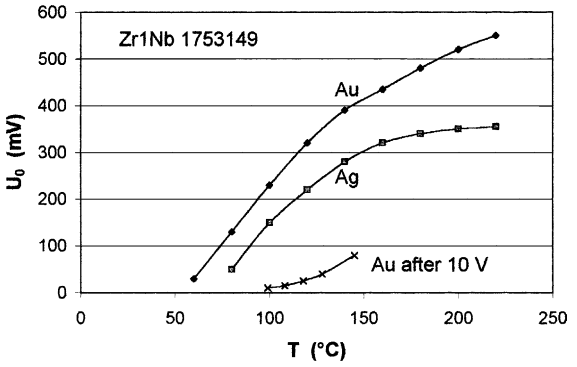

Fig. 8. Temperature dependence of the open-circuit voltage U_0 (sample Zr1Nb 1753149, Ag electrode) showing saturation at 360 mV, Au electrode with still rising U_0. The curve (after 10 V) with the low values of U_0 was measured after exposure to 220 °C and ±10 V.

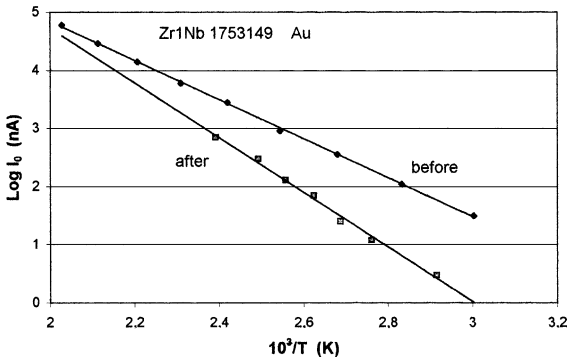

Fig. 9. Temperature dependence of short-circuit current I_0, Au electrode. Upper line before, and lower line after, exposure to 220 °C and ±10 V, respectively.

values of I_0 and U_0 remained constant, when the linear part of the I–V characteristics was measured with small voltages (max 1 V) up to 220 °C, exposure to ±10 V at 220 °C resulted in an irreversible decrease of more than an order of magnitude both for U_0 (Fig. 8) and I_0 (Fig. 9). Also the resistivity increased by half an order of magnitude, but with unchanged activation energy. The observed change remained permanent. Annealing at 120 °C for 72 h did not alter the diminished value.

3.3. Temperature dependence of the electric current and activation energy

The free carrier activation energy E is computed from the slope of the $\log \rho = f(1/T)$ straight line derived from the linear part of the temperature dependent current of the I–V characteristics. This was done by heating specimens in a temperature-controlled mini-thermostat, and measuring either the temperature-dependent currents at two different voltages in order to extricate the Ohmic part of conductivity, or by measuring the I–V characteristics at chosen constant temperatures and computing the resistivity from the linear part in the vicinity of the origin. The latter method was preferred. Figs. 10–12 are presented as an example of the first procedure. The values of the applied voltages U_1 and U_2 were chosen as low as possible in order to obtain prevailing Ohmic conduction and to reduce the influence of charge-limited currents, but high enough to ensure good current readings. In Fig. 13 both procedures are compared to show the pitfalls of measuring with continuously rising temperature. Here the rate of the temperature

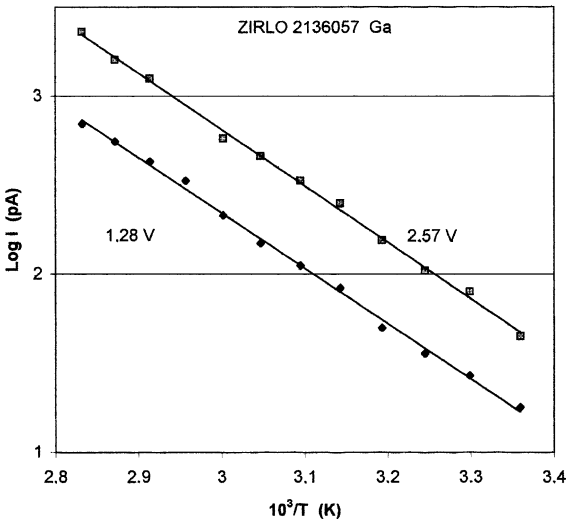

Fig. 10. Temperature dependence of current at two different voltages, measured at rising temperature 1 °C/min (ZIRLO 2136057, Ga-electrode). Fitted linear regression lines to smooth out measuring errors are used for computation of values shown in Figs. 11 and 12.

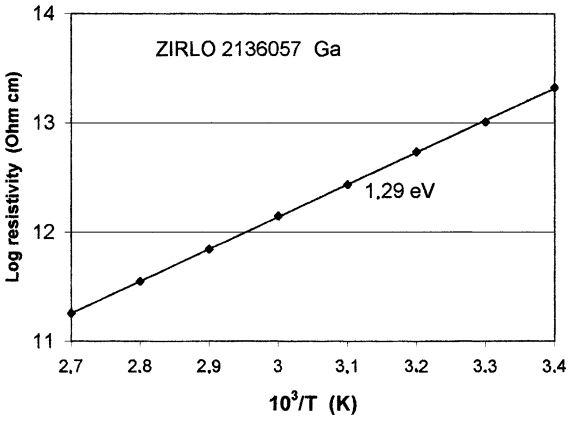

Fig. 11. Temperature dependence of resistivity, using values taken from Fig. 10.

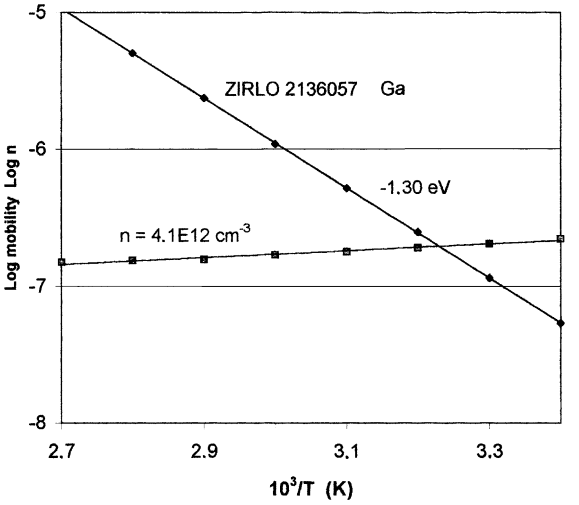

Fig. 12. Temperature dependence of carrier concentration n and mobility μ, using values taken from Fig. 10.

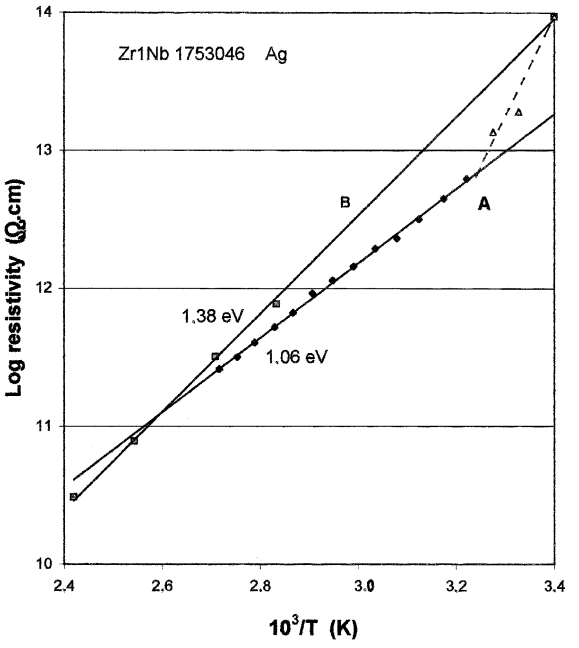

Fig. 13. Comparing results obtained A – at dynamic measurements at two voltages with too fast temperature rise, and B – static measurements of I–V characteristics at constant temperature and steady-state conditions. Prolongation of static straight line includes the equilibrium point at room temperature ($1/T = 3.4 \times 10^{-3}$). In A there is a systematic deviation because of too fast temperature rise, the resistivity is erroneously lower, especially near room temperature, where there was not enough time to reach the injection current limit. Both lines meet at high enough temperature, where steady-state conditions are reached for both procedures.

increase was too fast. The currents, especially at lower temperatures, were too high, owing to the non-finished injection currents and, accordingly, the computed resistivity was too low. At higher temperatures the injection currents decreased faster, and the computed resistivity approached the true values, which were computed from the I–V characteristics measured at constant temperatures and at equilibrium conditions. From the slope of the temperature-dependent resistivity line, the activation energy could be derived by using the exponential relationship.

$$1/\sigma = \rho = \rho_0 \exp(E/2kT),$$

or

$$\sigma = A \exp(-E/2kT). \tag{5}$$

For each oxidation/time there are two specimens, i.e. without and with evaporated gold electrodes. Although the specimens of each series were treated in identical manner, the results are somewhat different, demonstrating the range of measuring error and sample difference.

Although all specimens had nearly the same thickness, $w = (2.5 \pm 0.8)$ μm, there was a large difference in room temperature resistivity and activation energy values, depending on oxidation conditions. A pronounced influence of the electrode metal could be observed, contrary to Howlader et al. [3], who found no substantial differences in this respect. The specimens belonged to the first kind, where a hypostoichiometric layer at the metal–oxide interface is predominating (Cox et al. [6]). The oxide film is of dark colour and has relatively high conductivity (see Fig. 14). Remarkable is the high open-circuit voltage of over 200 mV at 100 °C of specimens oxidized in steam. On the contrary, the oxidation in water produced smaller values, as is seen for the last four double specimens in Table 3. The samples were first oxidized in water at 360 °C for 21 days, then in steam at 500 °C for 1 day, and finally in water for 1 day or 3 days. The measurements were repeated with vacuum evaporated gold electrodes, even though sprayed-on graphite is simpler and faster.

Table 4 gives results obtained with specimens of the second kind, i.e. with light coloured layers, thicker than 5 μm, where the white oxide of high resistivity is predominating (Cox et al. [6]).

In order to show a connection between resistivity and oxide layer thickness, the respective values contained in Tables 3 and 4 are plotted in Fig. 14. There can be seen a pronounced tendency of resistivity, especially of specimens of Zr1Nb of the first kind, to drop with slightly increasing thickness to very low values, with a power dependence of approximately $\rho \sim w^{-10}$. On the other hand, there exists a tendency of rising resistivity with increasing oxide layer thickness w for specimens of the second kind, with a power law of $\rho \sim w^3$. For the other

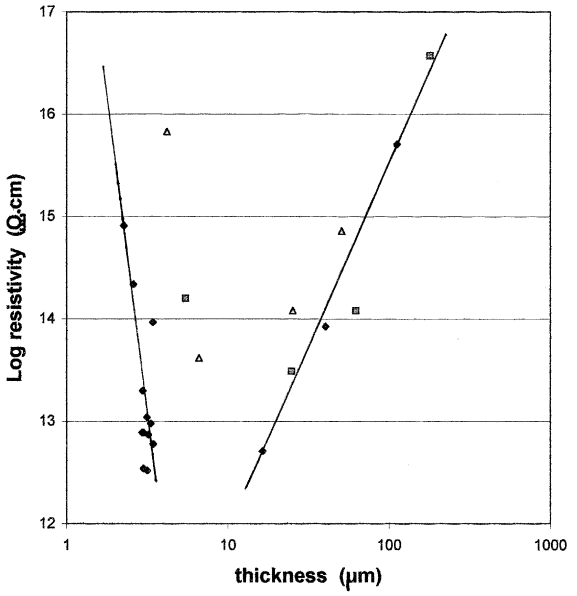

Fig. 14. Dependence of resistivity on oxide layer thickness. Layers of the first kind, with dark colour and small thickness (below 5 μm), have strongly decreasing resistivity $\sim w^{-10}$. Layers of the second kind, with light colour and large thickness (over 10 μm), have high resistivity, increasing with thickness $\sim w^3$. ◆: Zr1Nb, ■: ZIRLO, ▲: Zry- 4W.

alloys, ZIRLO and Zry-4W, an indication of similar tendency can be seen, but the number of samples is too small for arriving at any definite conclusion. This is in accordance with the findings of Cox et al. [6], who could show by metallographic investigation of thick oxide layers that the layers consist of a black, highly conductive hypostoichiometric layer next to the metal–oxide interface, and of a thicker, white layer near the surface of high resistivity. The $\rho = f(w)$ dependence in Fig. 14 then could be explained by varying contributions of the black and white oxide type.

It is plausible that when the oxide layer begins to grow, the black, highly conductive form below the white surface layer, develops slowly at first, and after reaching a certain thickness its growth rate diminishes, whereas the white, high resistive oxide continues to grow and predominates at larger thicknesses. Further confirmation of this hypothesis is given in Fig. 15, where the values of free carrier concentrations, computed from the second-order term of the I–V characteristics and contained in Tables 3 and 4, are plotted as a function of the oxide layer thickness. It can be assumed that the free carrier concentration n originates from oxygen vacancies acting as traps. The substoichiometric black layer near the metal–oxide interface remains nearly constant at subsequent growth of stoichiometric white oxide which is nearly without oxygen vacancies. Therefore the

Table 3
Observed values for Zr1Nb 1753 ... (dark coloured, thin layers of the first kind)

Sample	Oxidation[a] time (d)	w (μm)	Electrode	ε_r (–)	E (eV)	ρ_0 (Ω cm)	ρ_{20} (Ω cm)	U_0 (mV)
142	s	2.59	Ag	13.3	1.33	812	2.2×10^{14}	–
	1		Ga	14.5	1.15	3.3×10^4	2.5×10^{14}	–
149	Same	2.26	Au	20	1.5	46.7	8.1×10^{14}	230
133	s + w	2.93	Ag	25.5	0.79	1.3×10^6	1.3×10^{14}	–
	1 + 1		Ga	10?	–	–	–	–
			C	22	–	–	–	–
134	Same	2.96	Au	26	1.3	149	2×10^{13}	190
126	s + w	3.43	Ag	31.5	2.07	0.00127	7.1×10^{14}	210
	1 + 3		Ga	32	1.38	4.5	5.4×10^{13}	200
			C	–	1.49	14.5	9.4×10^{13}	300
127	Same	3.44	Au	33	1.0	1.5×10^4	6×10^{12}	240
045	w	1.83	C	25	0.15	6.1×10^8	1.2×10^{10}	3
	21							
046	Same	1.84	Au	–	–	–	–	–
041	w + s	3.17	C	23	0.8	4.4×10^5	3.3×10^{12}	2
	21 + 1							
040	Same	2.99	Au	33	1.0	1.4×10^4	7.8×10^{12}	8.3
035	w + s + w	3.21	C	23	0.79	1.2×10^6	7.4×10^{12}	4
	21 + 1 + 1							
033	Same	3.14	Au	19	0.98	4.1×10^4	1.1×10^{13}	11.2
027	w + s + w	3.33	C	21.5	0.87	3.2×10^6	9.5×10^{12}	9
	21 + 1 + 3							
025	Same	2.99	Au	23	0.77	8×10^5	2.5×10^{12}	32

[a] Oxidation: w (water at 360 °C), s (steam at 500 °C).

Table 4
Observed values for Zr1Nb, ZIRLO and Zry-4W (light coloured, thick layers of the second kind, Ga and Ag electrodes)

Sample	Oxidation[a] time (d)	w (μm)	ε_r (–)	E (eV)	ρ_0 (Ω cm)	ρ_{20} (Ω cm)	n (cm^{-3})	μ_{20} (cm^2/V s)
Zr1Nb 1136057	w	16.5	27	1.25	98.7	5.1×10^{12}	4.6×10^{14}	5.7×10^{-8}
ZIRLO 2136057	w	24.9	29	1.28	381	3.1×10^{13}	4.5×10^{12}	3.1×10^{-8}
Zry-4W 3136057	w	25.3	22	1.22	3993	1.2×10^{14}	4.4×10^{13}	1.9×10^{-9}
Zr1Nb 1240013	s	40.3	27	1.35	235	8.6×10^{13}	1.6×10^{13}	4.2×10^{-9}
ZIRLO 2240013	s	62.2	23	1.65	0.729	1.2×10^{14}	1.3×10^{12}	1.4×10^{-9}
Zry-4W 3240013	s	24.2	22	1.28	1.15×10^{6}	6.7×10^{15}	9.2×10^{12}	1×10^{-10}
Zr1Nb 1245023	s 630	111.9	22	1.83	0.697	5×10^{15}	1.9×10^{12}	7.8×10^{-9}
ZIRLO 2245030	s 462	179.6	17	2.05	0.109	3.7×10^{16}	3.4×10^{11}	2.3×10^{-9}
Zry-4W 3245062	s 38.6	50.7	53	1.4	672	7.3×10^{14}	1×10^{12}	1.8×10^{-9}
ZIRLO 2336027	70 ppm Li	5.46	21	1.86	0.0169	1.6×10^{14}	6×10^{13}	4.2×10^{-10}
Zry-4W 3336027	70 ppm Li	6.61	17	1.29	348	4.2×10^{13}	2.3×10^{13}	8.5×10^{-9}

[a] Oxidation: w (water at 360 °C), s (steam at 400 and 450 °C, respectively), 70 ppm Li^+ (water + $LiCO_3$, 360 °C).

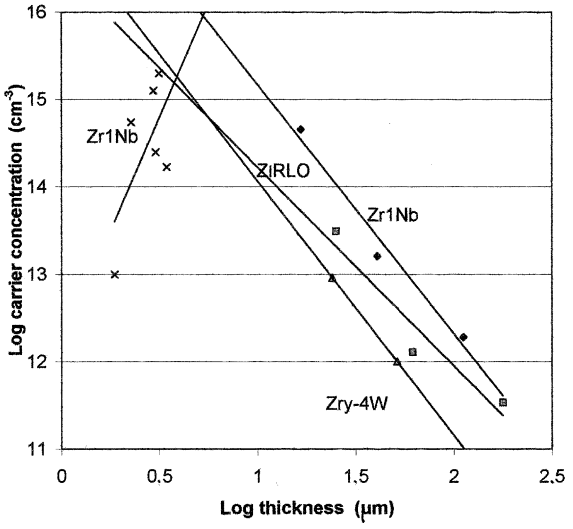

Fig. 15. Mean carrier concentration n computed using coefficient a of second-order polynomial of I–V characteristics (Eq. (4)) plotted against the oxide layer thickness w. (Thin layers of Zr1Nb only.)

number of carriers remains almost constant, but is distributed at larger layer thicknesses over a larger volume, thereby decreasing the mean carrier concentration shown in Fig. 15. The power law dependence $n \sim w^{-3}$ for Zr1Nb samples corresponds well to $\rho \sim w^3$ of the same samples in Fig 14, implicating a nearly equal carrier mobility at room temperature. The number of ZIRLO and Zry-4W samples is too small to insert lines of linear regression for meaningful conclusions.

3.4. Confirmation of the Meyer–Neldel rule (MNR)

Since ZrO_2 is a high-resistivity oxidic semiconductor, it is reasonable to expect that the MNR would apply. Meyer and Neldel [15] found that the experimentally assessed temperature-dependent conductivity of high-resistivity semiconductors, whose conductivity is lower than 0.01 S/cm and activation energy $E \gg kT$, obeys a simple relationship between activation energy and pre-exponential factor.

According to Yelon et al. [16], who described the origin and consequences of the compensation (Meyer–Neldel) law, the MNR applies to groups of related activated processes (electronic processes in amorphous semiconductors, trapping in crystalline semiconductors, conductivity in ionic conductors, annealing processes, etc.) for which a measured property X is given by

$$X = A \exp(-E/kT). \tag{6}$$

When the activation energy E varies, the pre-exponential factor A obeys the equation

$$\ln A = \alpha + \beta E, \tag{7}$$

which is the MNR, as described in [15,16]. Here α and β are positive constants, characteristic for the semiconductor in question. The activation energy E is not a material constant, in fact it is determined by the energy difference between the lattice defects and the lower edge of the conduction band. In Fig. 16 the observed activation energies E for the series of specimens, listed in Tables 3 and 4, are plotted as a function of $\ln A$, where $A = 1/\rho_0$ is the pre-exponential factor in the exponential temperature dependence of conductivity/resistivity. Although A spans a wide range of 12 orders of magnitude, the experimental values of E for Zr1Nb follow a straight line.

The observed values of ZIRLO and Zry-4W alone lie almost on the same straight line, but are too few for separate MNR lines.

The constant α is a complex function of several variables including the defect formation energy, oxygen pressure, electron mobility, etc. The interpretation of β is simpler:

$$\beta = e/2kT_0. \tag{8}$$

The slope of the straight line in Fig. 16 is 14.9 ± 0.04, so that $T_0 = 388$ K (115 ± 10 °C). Of higher importance, however, is the isokinetic energy $E_0 = kT_0 = 33$ meV.

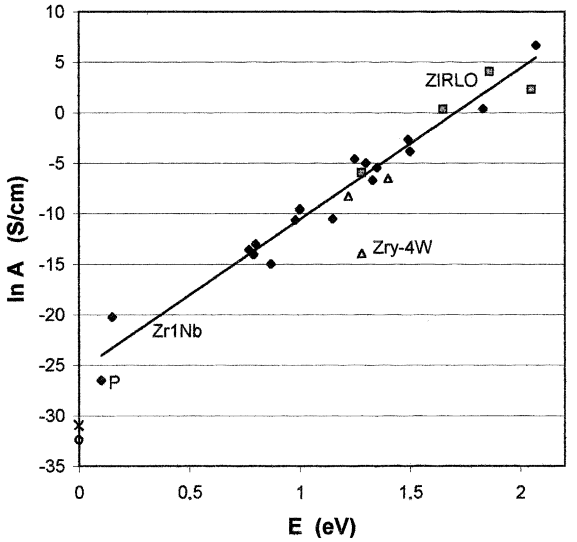

Fig. 16. Confirmation of the MNR. The logarithm of the pre-exponential factor A is a linear function of the activation energy E. Full line for Zr1Nb. Samples of ZIRLO and Zry-4W would give similar slopes, but are too few for exact evaluation. Point P taken from Fig. 3 of Ref. [3] is added, confirming the MNR [15]. The points O for Zircaloy-2, and X for Zircaloy-4 are lying outside the MNR for our samples, which may be due to different alloy composition.

The observed differences of resistivity and activation energy obtained with different electrode metals remain an open question. Although the results of Howlader et al. [3] were not influenced by the choice of the electrode metal, Cox [5] found a definite influence of electrode metals. At very low activation energies, as in the specimens of [3], the work function of the electrode metal is of minor importance, but at samples with higher activation energies the work function of the electrode metal will influence the carrier injection. This means that a potential step exists at the metal–oxide interface which will influence the current flow.

The importance of the MNR consists in the fact that different electrode metals, giving different values of activation energy and resistivity on the same specimen, will nevertheless have points lying on the same MNR straight line with common isokinetic energy.

The MNR implies that all specimens possess the same conductivity at the isokinetic temperature T_0 [16], and all lines of the temperature-dependent conductivity intersect in that point. This behaviour, called the isokinetic rule, has been known to chemists since 1929 [17]. The measured straight lines of $\log \rho = f(1/T)$ plotted together show indeed intersection at the isokinetic temperature in the vicinity of 100–120 °C.

Yelon et al. [16] investigated the origin of the MNR and found that the compensation law, Eq. (7), follows if the activation entropy is proportional to the activation enthalpy.

Surprising is the wide range of activation energy values, 0.15–2 eV in this study, which is probably due to the varying oxygen concentration in the oxide layer. Howlader et al. [3] reported very low activation energies from measurements in vacuum, which may be the cause of reduced oxygen contents. Charlesby [8] observed energies from 0.03 to 0.06 eV for reduced stabilized zirconia at low temperatures. At higher temperatures [3] the energy increased, reaching about 1 eV.

The activation energy of Improved Zircaloy-2, as taken from Fig. 3 in [3], is about 0.11 eV, which gives $A = 3 \times 10^{-12}$ S/cm for a conductivity of about 3×10^{11} S/m, fitting adequately our MNR straight line in Fig. 16 (Point P). Zircaloy-2, and Zircaloy-4 have zero activation energies at room temperature, and a conductivity of about 2×10^{-14} S/cm or $\ln A = -31.5$, and 4.5×10^{-14} S/cm or $\ln A = -30.7$, respectively. The pertaining points are lying somewhat outside our NMR straight line which may be due to a different composition of the alloys. The observed hysteresis of the conductivity may be due to the variation of the oxygen in the zirconium oxide matrix during measurements inside the bell jar, producing a very low value of A, which is also called the quantity factor (Mengenkonstante in [15]) because it involves the concentration of active lattice defects.

It is conceivable that above the critical temperature T_0 (115 °C in our case), changes in the lattice defect

concentration may take place due to the effect of oxygen when performing the measurements in open air. Therefore at first our measurements were limited to 100 °C, so as not to endanger the state of the existing frozen-in lattice defects. Nevertheless measurements up to 220 °C in air did not seem to change the behaviour of the samples as long as no higher voltage was applied, to measure the I–V characteristics, was applied. But at 10 V currents, the resistivity irreversibly increased by half an order of magnitude, and the open-circuit voltage U_0 was lowered (Figs. 8 and 9). In order to investigate the influence of non-stoichiometric oxygen contents in our specimens, annealing experiments in oxidizing and reducing atmospheres at temperatures up to the original oxidation temperature are planned. Merino and Orera [20] showed that thermochemically reduced zirconia stabilized with yttria developed an electronic conduction at low temperatures due to intrinsic electron traps.

In addition to the oxygen-vacancy complexes, there is a certain probability that the alloying elements will act as donor or trap centres. Inagaki et al. [7] mentions the possible influence of alloying additions. We had a sample of Zry-4W on which there was a brown tarnished spot of irregular form of about 10 mm^2 area, which was probably due to iron oxide contamination in the autoclave. Measurements at the clean surface showed a resistivity of 6.7×10^{15} Ωcm at room temperature with activation energy of 1.28 eV, whereas at the brown spot the values were as low as 8.7×10^{10} Ωcm and 0.57 eV, respectively.

4. Conclusions

It has been demonstrated that the electric current decrease on the application of potential to electrodes on the oxide layers of tubes made of zirconium alloys is due to injection currents building up a space charge which can be extracted again as short-circuit current with a hyperbolic time decrease. This space charge is a linear function of the applied voltage. Due to the space charge formed, the current in the equilibrium state is space-charge limited, obeying Child's law. The total current is composed of a linear, Ohmic part, and of a non-linear part, increasing with the applied voltage squared, and sometimes of a constant part of short-circuit current. The I–V characteristics are therefore non-linear, with a stronger curvature for the negative polarity at the zirconium electrode. The sense of the small rectification effect gives evidence of the electronic nature of the conduction process. Neither the $\log I = f(U^{1/2})$ plot nor the $\log I/U = f(U^{1/2})$ plot was linear, as would be expected for the Schottky emission model and the Poole–Frenkel effect, respectively. This confirms the dominance of space-charge limited currents at higher voltages, prevailing over the linear, Ohmic part of the current which dominates at lower voltages. A small fraction of the current is ionic in nature and manifests itself at higher temperatures by the existence of short-circuit current and open-circuit voltage with the result that the I–V characteristics do not pass through the origin. The conductivity/resistivity must be calculated from the linear part of the temperature-dependent I–V characteristics. Plotting the activation energy E against the logarithm of the pre-exponential factor A in the exponential relation for conductivity, a straight line is obtained, confirming the MNR. From the slope of the MNR line the isokinetic temperature $T_0 = 115$ °C was derived.

The oxide films are not homogeneous, but consist of a substoichiometric black oxide layer of high conductivity near the metal–oxide interface, and of an almost stoichiometric white layer of high resistivity [6]. At larger film thicknesses the high resistivity layer is dominating. The competition of both layer types produces a conductivity maximum for layers about 5 μm thick. Fully oxidized colourless layers are of monoclinic structure, whereas substoichiometric black layers with oxygen deficiency can have a tetragonal structure [21]. Moreover, part of the layer near the surface can be porous [6] so that sprayed-on electrode material could enter into the pores and alter the effective thickness of the layers. The relative permittivity computed from capacitance measurements of specimens of different electrode metals often deviated from the accepted value of $\varepsilon_r = 22$ for bulk zirconium oxide. This may be due partly to porosity of the layers or to wetting difficulties of the contacts, or to inhomogeneities of the layers [6]. Oxidation in aqueous surroundings leads to the development of hydrogen which can enter the bulk and when the terminal solubility limit is reached hydrides precipitate. The mechanical properties of Zircaloy are degraded when hydrides are present in the metal [18]. Hydrogen present in the oxide can form an impurity level in the band gap [19].

As a final result it can be concluded that zirconium oxide is an electronic high-resistivity semiconductor with extremely low, but with temperature increasing, mobility. The oxide layers of the specimens were inhomogeneous, consisting of a substoichiometric part of a black layer of relatively high conductivity near the metal-oxide interface, and of a lightly coloured stoichiometric part near the surface of high resistivity. The completion of the two types of layer composition leads to a maximum in conductivity for layers about 5 μm thick (Fig. 14). The relatively high electron concentration is independent of temperature and originates from oxygen vacancies existing predominatingly near the metal–oxide interface. The current is space-charge limited and the conduction mechanism is assumed to be a hopping process of electrons between oxygen vacancy traps. Also there exists a low ionic conduction part. The MNR is obeyed.

Acknowledgements

Support of this research by ŠKODA-ÚJP, Praha company is highly appreciated. Special thanks are due to Ms Věra Vrtílková for providing of oxidized specimens of specified thickness. We also thank Dr E. Hulicius of the Physical Institute of the AV CR for the evaporation of gold contacts, and Ms I. Dvorakova, Prom.Phil. for checking the manuscript.

References

[1] D.G. Franklin, P.M. Lang, C.M. Eucken, A.M. Garde (Eds.), Proc. 9th Int. Symp. Nucl. Industry, ASTM, Philadelphia, 1991, p. 3, ASTM STP 1132.
[2] Corrosion of Zirconium Alloys in Nuclear Power Plants, IAEA-TECDOC-684, Vienna 1993.
[3] M.M.R. Howlader, K. Shiiyama, C. Kinoshita, M. Kutsuwada, M. Inagaki, J. Nucl. Mater. 253 (1998) 149.
[4] S.J. Lee, E.A. Cho, S.J. Ahn, H.S. Kwon, Electrochim. Acta 46 (2001) 2605.
[5] B. Cox, J. Nucl. Mater. 37 (1970) 177.
[6] B. Cox, Y.-M. Wong, J. Mostaghimi, J. Nucl. Mater. 226 (1995) 272.
[7] M. Inagaki, M. Kanno, H. Maki, ASTM STP 1132 (1992) 437.
[8] A. Charlesby, Acta Metall. 1 (1953) 348.
[9] T.E. Hartman, J.C. Blair, R. Bauer, J. Appl. Phys. 37 (1966) 2468.
[10] N.F. Mott, R.W. Guerney, Electronic Processes in Ionic Crystals, Clarendon, Oxford, 1940.
[11] A. Rose, Phys. Rev. 97 (1955) 1538.
[12] J.G. Simmons, Phys. Rev. 155 (1967) 657.
[13] C.A. Mead, Phys. Rev. 128 (1962) 2088.
[14] P.J. Shirvington, J. Nucl. Mater. 50 (1974) 183.
[15] W. Meyer, H. Neldel, Z. Techn. Phys. 12 (1937) 588.
[16] A. Yelon, B. Mowaghar, H.M. Branz, Phys. Rev. B 46 (1992) 12244.
[17] G.M. Schwab, Z. Phys. Chem. 58 (1929) 406.
[18] M. Oskarsson, E. Ahlberg, U. Sodervall, U. Andersson, K. Pettersson, J. Nucl. Mater. 289 (2001) 315.
[19] M. Okui, T. Nishizaki, M. Uno, K. Kurosaki, S. Yamanaka, K. Takeda K, H. Anada, J. Alloys Compd. 330–332 (2002) 645.
[20] R.I. Merino, V.M. Orera, Solid State Ionics 76 (1995) 97.
[21] K. Koski, J. Holsa, P. Juliet, Surf. Coat. Technol. 120&121 (1999) 303.